REPORT DOCUMENTATION PAGE

Form Approved OMB NO. 0704-0188

1. REPORT DATE (DD-MM-YYYY)	2. REPORT TYPE	3. DATES COVERED (From - To)
22-09-2021	Final Report	15-Jun-2020 - 14-Sep-2021

4. TITLE AND SUBTITLE

Final Report: The Role of Chemical and Structural Disorder at Buried Interfaces in Hexaferrite Heterostructures: Implications to Microwave Integrated Electronics

5a. CONTRACT NUMBER
W911NF-20-1-0069

5b. GRANT NUMBER

5c. PROGRAM ELEMENT NUMBER
611102

6. AUTHORS

5d. PROJECT NUMBER

5e. TASK NUMBER

5f. WORK UNIT NUMBER

7. PERFORMING ORGANIZATION NAMES AND ADDRESSES

Northeastern University
360 Huntington Avenue
490 RP
Boston, MA 02115 -5005

8. PERFORMING ORGANIZATION REPORT NUMBER

9. SPONSORING/MONITORING AGENCY NAME(S) AND ADDRESS (ES)

U.S. Army Research Office
P.O. Box 12211
Research Triangle Park, NC 27709-2211

10. SPONSOR/MONITOR'S ACRONYM(S)
ARO

11. SPONSOR/MONITOR'S REPORT NUMBER(S)
76775-MS-II.2

12. DISTRIBUTION AVAILIBILITY STATEMENT

Approved for public release; distribution is unlimited.

13. SUPPLEMENTARY NOTES

The views, opinions and/or findings contained in this report are those of the author(s) and should not contrued as an official Department of the Army position, policy or decision, unless so designated by other documentation.

14. ABSTRACT

15. SUBJECT TERMS

16. SECURITY CLASSIFICATION OF:			17. LIMITATION OF ABSTRACT	15. NUMBER OF PAGES	19a. NAME OF RESPONSIBLE PERSON
a. REPORT	b. ABSTRACT	c. THIS PAGE			Vincent Harris
UU	UU	UU	UU		19b. TELEPHONE NUMBER 617-373-7603

RPPR Final Report
as of 23-Sep-2021

Agency Code: 21XD

Proposal Number: 76775MSII **Agreement Number: W911NF-20-1-0069**
INVESTIGATOR(S):

Name: Ph.D. Vincent Gerard Harris
Email: harris@ece.neu.edu
Phone Number: 6173737603
Principal: Y

Name: Ph.D. Ogheneyunume Fitchorova
Email: o.obi@northeastern.edu
Phone Number: 7812388436
Principal: N

Organization: **Northeastern University**
Address: 360 Huntington Avenue, Boston, MA 021155005
Country: USA
DUNS Number: 001423631 EIN: 104167998

Report Date: 14-Dec-2021 Date Received: 22-Sep-2021
Final Report for Period Beginning 15-Jun-2020 and Ending 14-Sep-2021

Title: The Role of Chemical and Structural Disorder at Buried Interfaces in Hexaferrite Heterostructures: Implications to Microwave Integrated Electronics
Begin Performance Period: 15-Jun-2020 **End Performance Period:** 14-Sep-2021
Report Term: 0-Other

Submitted By: Ph.D. Vincent Harris Email: harris@ece.neu.edu
Phone: (617) 373-7603

STEM Degrees: 0 **STEM Participants:** 1

Major Goals: The main objective of this program was the systematic study to establish fundamental interrelationships in the processing-structure-property paradigm in the epitaxial growth of hexaferrites on wide bandgap substrates with proper strain-mediating buffer layers. These findings provide a viable path to the development of next generation magnetic mm-wave devices that are planar and low-loss and monolithically integrated with active semiconductor device platforms.
Objective 1: To explore the interrelationships between thin film growth dynamics (i.e., pulsed laser energy and density, substrate temperature, background pressure, component geometries) and fundamental (atomic and electronic structure and defects) and functional properties (i.e., magnetization, coercivity, retention, permeability, permittivity and related losses) as they pertain to the performance of materials and rf passive devices operating at mm-wavelengths (i.e., insertion loss, isolation, return loss). Principle characterization techniques include x-ray diffraction and electron microscopy, including high-resolution transmission electron microscopy.
Objective 2: To explore the interrelationships between film growth dynamics upon the properties of interfaces formed at the boundary of substrate and nucleation layers, and nucleation layers and the magnetodielectric film (i. e., hexaferrite). Such techniques as cross-sectional HR-TEM to quantitatively investigate the structural, chemical and defect properties of the interfacial region.

Accomplishments: See attached pdf with figures

Training Opportunities: One RA received extensive training in the use of PLD, microwave characterization, and electron microscopy.

Dr. Parisa Andalib received extensive training in mentoring and training the RA under the tutelage of the PI, Prof. Harris

RPPR Final Report
as of 23-Sep-2021

Results Dissemination:
Special Issue on 5G Materials

C. Yu, P. Andalib, A. Sokolov, O. Fitchorova, W. Liang, E. Beam, and V.G. Harris, “Interface-engineered barium magnetoplumbite – wide-bandgap semiconductor integration enabling 5G system-on-wafer solutions for full-duplexing phased arrays,” Appl. Phys. Lett., 119, 051906 (2021); doi: 10.1063/5.0058784

Invited Presentation

V.G. Harris, “Interface-engineered barium hexaferrite – wide-bandgap semiconductor integration enabling 5G system-on-wafer solutions," Front Range Advanced Magnetics Symposium, Ft. Collins, CO, Sept, 18-19, 2021.

V.G. Harris, “Interface-engineered barium hexaferrite – wide-bandgap semiconductor integration enabling 5G system-on-wafer solutions," IEEE Intermag, New Orleans, Jan. 22, 2022

Honors and Awards: V.G. Harris
Elevated to senior member of the National Academy of Inventors (2020)
Jefferson Science Fellow, Department of State (2020-2021)
Fulbright Specialists Program, European Union (2020-2022)

Protocol Activity Status:

Technology Transfer: Nothing to Report

PARTICIPANTS:

Participant Type: PD/PI
Participant: Vincent G Harris
Person Months Worked: 1.00 **Funding Support:**
Project Contribution:
National Academy Member: N

Participant Type: Co PD/PI
Participant: Ogheneyunume Fitchorova
Person Months Worked: 1.00 **Funding Support:**
Project Contribution:
National Academy Member: N

Participant Type: Staff Scientist (doctoral level)
Participant: Parisa Andalib
Person Months Worked: 1.00 **Funding Support:**
Project Contribution:
National Academy Member: N

Participant Type: Graduate Student (research assistant)
Participant: Chengju Yu
Person Months Worked: 2.00 **Funding Support:**
Project Contribution:
National Academy Member: N

RPPR Final Report
as of 23-Sep-2021

ARTICLES:

Publication Type: Journal Article Peer Reviewed: Y **Publication Status:** 1-Published
Journal: Applied Physics Letters
Publication Identifier Type: DOI Publication Identifier: 10.1063/5.0058784
Volume: 19 Issue: 5 First Page #: 051906
Date Submitted: 9/15/21 12:00AM Date Published: 8/6/21 8:00AM
Publication Location: Melville, NY USA
Article Title: Interface-engineered barium magnetoplumbite–wide-bandgap semiconductor integration enabling 5G system-on-wafer solutions for full-duplexing phased arrays
Authors: Chengju Yu, Parisa Andalib, Alexander Sokolov, Ogheneyunume Fitchorova, Wentao Liang, Edward Be
Keywords: Antennas Radio spectrum Pulsed laser deposition Semiconductors Interface diffusion Multiple input multiple output Ferromagnetic materials Magnetic anisotropy
Abstract: Transition from fourth to fifth generation wireless technologies requires a shift from 2.3?GHz to Ka-band with the promise of revolutionary increases in data handling capacity and transfer rates at greatly reduced latency among other benefits. A key enabling technology is the integration of Ka-band massive multiple input–multiple output (m-MIMO) antenna arrays. m-MIMO array elements simultaneously transmit and receive (STAR) data providing true full duplexing in time and frequency domains. STAR requires, as a central component, the circulator. Here, we report results of a systematic study of pulsed laser deposited (PLD) barium magnetoplumbite (BaM) films on industrial compatible WBG semiconductor heterostructures suitable for operation in Ka-band circulators. We demonstrate successful PLD growth of BaM films on WBG semiconductor heterostructures. BaM films that show device quality performance in structure, epitaxy, and magnetic properties were realized for BaM/MgO/AlN/SiC(X).
Distribution Statement: 2-Distribution Limited to U.S. Government agencies only; report contains proprietary info
Acknowledged Federal Support: **Y**

Partners

,

Wentao Liang (KRI at Northeastern), Research Scientist, TEM assistance.Alex Sokolov, NEU, Post-doc, growth ass

I certify that the information in the report is complete and accurate:
Signature: Vincent G Harris
Signature Date: 9/22/21 11:08AM

Topic Title: The Role of Chemical and Structural Disorder at Buried Interfaces in Hexaferrite Heterostructures: Implications to RF Microwave Integrated Electronics

Federal Awarding Agency: Army Research Office (ARO)

ARO Grants Officer's Representative:

Dr. Chakrapani V. Varanasi, chakrapani.v.varanasi.civ@army.mil, (919) 549-4325

Address: US ARMY ACC-APG-RTP W911NF

800 Park Office Drive, Suite 4229

Research Triangle Park NC 27709

Federal Award No: W911NF-20-1-0069

Principal Investigator: Northeastern University

PI: Vincent Harris Ph.D., 617-373-7603, harris@ece.neu.edu

Address: 360 Huntington Ave, Boston, MA 02115-5005

Subcontractor: KRI at Northeastern University, LLC

Technical Point of Contact: Ogheneyunume Fitchorova Ph.D., 781-238-8436, y.obi@kri.neu.edu

Address: 141 South Bedford St., Burlington, MA 01803-2736

Table of Contents

Executive Summary 3
Project Objective 4
Project Approach 4
Results and Analysis ..... **Error! Bookmark not defined.**
Conclusions 14
References 14
Appendix A: Supplemental Data 16

Executive Summary

In this STIR program we investigated fundamental interrelationships in the processing-structure-property paradigm of epitaxial grown hexaferrites on wide bandgap substrates and demonstrated successful PLD growth of *BaM* films on WBG semiconductor heterostructures. Device quality performance in structure (as seen in Figure 1), epitaxy, and electromagnetic performance were realized for BaM/MgO/AlN/SiC(X) heterostructures. Film properties include bulk-like values of magnetic anisotropy field, $H_a \sim 16.5$ kOe, and saturation magnetization, $4\pi M_s \sim 4.2$ kG. FMR linewidth values are competitive and comparable with device design goals for insertion loss. Only heterostructures where SiC substrates having Si-polar surfaces showed superior properties whereas C-polar surfaces gave rise to high and detrimental average surface roughness leading to a deterioration in RF performance. Overall, hysteresis loop squareness values remained low for self-bias applications. These results define a path for integration of magnetodielectric materials on wide bandgap heterostructures essential to the realization of a transmit-receive system on wafer (SoW) topology necessary for the development of 5G Ka-band massive multiple input – multiple output (*m-MIMO*) antenna arrays with true full duplexing in time and frequency domains.

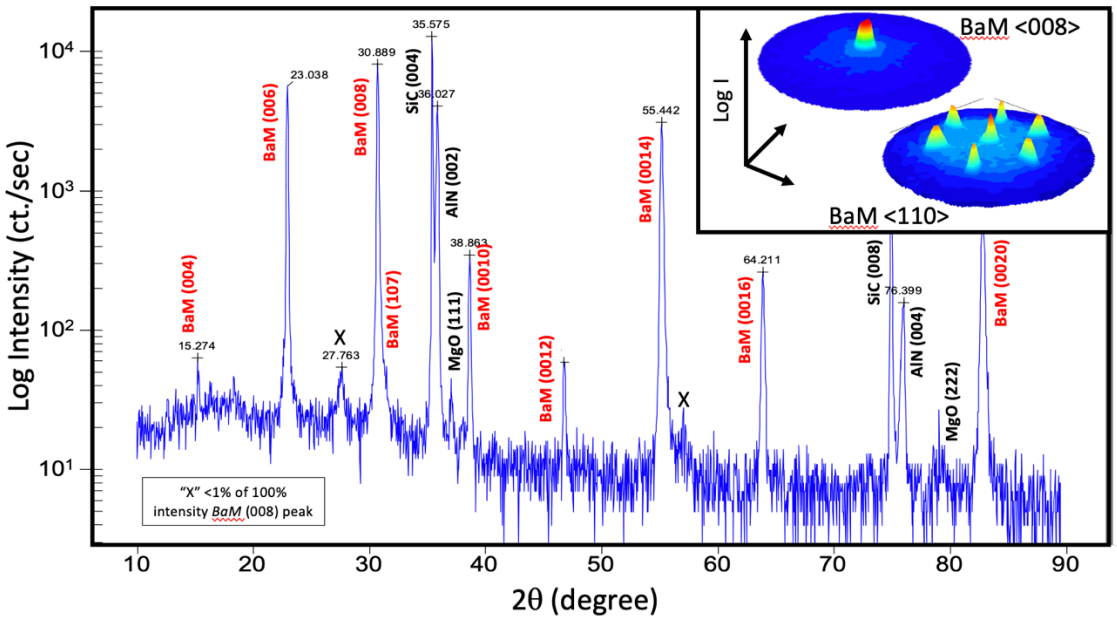

Figure 1. **Room temperature, $\theta - 2\theta$ x-ray diffraction spectrum (Cu Kα-radiation source), as the logarithm of intensity, for a BaM/MgO/AlN/SiC(X) heterostructure. Diffraction peaks are indexed to (00l) reflections of the BaM film with some high intensity peaks attributed and labeled to the substrate, capping layer (AlN) and nucleation layer (MgO). The inset image is of two pole figures confirming epitaxy <008>, and the 6-fold symmetry and in-plane registry <110> of hexagonal crystals. X in the main panel identifies peaks below the 1% threshold, relative the BaM (008) intensity, that are unidentified but may arise from alloys formed at interface diffusion regions.**

Federal Award No: W911NF-20-1-0069

Project Objective

The main objective of this program was the systematic study to establish fundamental interrelationships in the processing-structure-property paradigm in the epitaxial growth of hexaferrites on wide bandgap substrates with proper strain-mediating buffer layers. These findings provide a viable path to the development of next generation magnetic mm-wave devices that are planar and low-loss and monolithically integrated with active semiconductor device platforms.

Objective 1: To explore the interrelationships between thin film growth dynamics (i.e., pulsed laser energy and density, substrate temperature, background pressure, component geometries) and fundamental (atomic and electronic structure and defects) and functional properties (i.e., magnetization, coercivity, retention, permeability, permittivity and related losses) as they pertain to the performance of materials and rf passive devices operating at mm-wavelengths (i.e., insertion loss, isolation, return loss). Principle characterization techniques include x-ray diffraction and electron microscopy, including high-resolution transmission electron microscopy.

Objective 2: To explore the interrelationships between film growth dynamics upon the properties of interfaces formed at the boundary of substrate and nucleation layers, and nucleation layers and the magnetodielectric film (i.e., hexaferrite). Such techniques as cross-sectional HR-TEM to quantitatively investigate the structural, chemical and defect properties of the interfacial region.

Project Approach

Transition from fourth to fifth generation wireless technologies requires a shift from 2.3 GHz to Ka-band with the promise of revolutionary increases in data handling capacity and transfer rates at greatly reduced latency among other benefits. A key enabling technology is the integration of Ka-band *m-MIMO* antenna arrays. *m-MIMO* array elements simultaneously transmit and receive (STAR) data providing true full duplexing in time and frequency domains. STAR requires, as a central component, the circulator. However, conventional circulators are bulky and prohibit the engineering of Ka array lattices. A necessary innovation calls for the integration of device-quality Ka-ferrites with wide bandgap (WBG) semiconductor heterostructures allowing for system-on-wafer solutions.

A practical integration has not yet been achieved due to several technical challenges that primarily involve the interfaces between layers of different materials in ferrite/semiconductor heterostructures. For example, despite having a similar hexagonal crystal structure, these semiconductor materials still experience large atomic lattice mismatches giving rise to strain and copious related defects. Additionally, interdiffusion at the interface may degrade the quality and performance of the ferrite and semiconductor. Further degradation may result from the residual strain and related defects originating from dissimilar thermal expansion coefficients.

A careful study of the interfaces in hexaferrite heterostructures may address and resolve most of these challenges. For example, an unacceptable lattice mismatch of 5% between commonly used

barium hexaferrites and gallium nitrides can be reduced to under 2% by employing an interlayer (i.e., buffer layer) of magnesium oxide (MgO). Such interlayers can also act as a barrier to minimize interdiffusion. Finally, a layer of aluminum nitride can be employed to reduce residual stress. In previous studies by the Harris Team (Chen, et al., 2012) the growth of BaM films on GaN/sapphire were explored. They demonstrated that the degree of interface interdiffusion can be directly correlated with the hysteresis behavior. A recent paper published by the team presents a complete investigation of the impact of laser process conditions on ferrite film structure and properties when grown on wide bandgap substrates (Yu, et al., 2020). The growth of ferrites on semiconductors is a topic not well studied. In more recent years, the Harris Team has made great progress in the processing of high-quality ferrite films on semiconductor substrates by sputtering, screen printing, PLD, MBE, LPE, and wafer bonding. Of these studies, the use of PLD has been found to be the most cost-effective technique to produce ferrite films of suitable quality for RF applications.

Major tasks undertaken in this program are as below:

Task 1: PLD Growth of substituted Barium Hexaferrites – Wide Bandgap Heterostructures

In Task 1, we explore the interrelationships between thin film growth parameters (i.e., pulsed laser energy and density, substrate temperature, background pressure, substrate - target geometries) and film properties. Film properties include surface roughness, crystallographic texture, crystal morphology, magnetization, Curie temperature, coercivity, magnetic anisotropy field, and hysteresis retention (or squareness). Additionally, RF properties including FMR linewidth, and complex permeability and permittivity will be measured over frequencies encompassing Ka-band.

Task 2: Characterization of the Chemistry, Structure and Defects of Buried Interfaces

Ultimately, the nature of the interface dictates the functional properties of these devices. Here, we will employ cross sectional HR-TEM to image the interfaces between the GaN on SiC substrate and the buffer layers (MgO and AlN) and the buffer layer (MgO and AlN) and the BaM hexaferrite. The degree of interdiffusion, stacking fault density, and roughness at the interface will be ascertained. These interface properties will be controlled and optimized by tailoring interfacial strain.

Task 3: Correlation of measured interface properties with functional properties

A key element of this STIR program is the measurement and correlation of interfacial properties with the functional properties of the hexaferrite films on wide bandgap heterostructures and derived devices. To this end, the properties deduced from Task 2 will be correlated with the findings of Task 1 to establish causal relationships allowing for the optimized growth of high-quality ferrite materials on wide bandgap heterostructures.

Accomplishments

Task 1: PLD Growth of substituted Barium Hexaferrites – Wide Bandgap Heterostructures

All substrate heterostructures reported here are of the form BaM/NL/WBG-CL/SiC(X), where NL denotes nucleation layer, WBG-CL is the wide bandgap capping layer (i.e., here GaN or AlN), and X indicates that the 6H-SiC substrate is a single crystal. In some cases, the termination of the SiC, be it C-polar vs. Si-polar, was also explored. The growth of the WBG capping layers was performed using metalorganic chemical vapor deposition (MOCVD) following the protocols of ref. 3, while nucleation layers of MgO and Pt were grown by atomic layer deposition (ALD, Ultratech Fiji plasma-assisted ALD reactor). Pt nucleation layers of 20 nm, with an average surface roughness of 0.43 nm, were deposited at 250 ^{o}C with (111) crystal texture. Similarly, MgO nucleation layers of 32 nm, with an average surface roughness of 0.31 nm, were deposited at 325 ^{o}C with (111) crystal texture. As representative of film quality, the FWHM of the MgO (222) was 1000 arcsec.

BaM films were pulsed laser deposited using a KrF excimer laser operating at 248 nm generating 10 ns pulses at a rate of 10 Hz. Laser pulses were incident upon a pure phase 25 mm diameter *BaM* target at a 45^{o} angle in a dynamic vacuum of 26.6 Pa (or 200 mTorr) of oxygen partial pressure. The laser plume was intercepted by a substrate holder held at 920 ^{o}C. The substrate holder, which also served as a resistive heater, was aligned parallel to the target at a distance of 70 mm. The laser beam remained fixed while the target was rotated at 30 rpm and rastered relative to the incident laser beam in order to ensure a homogeneous and uniform films. The substrate surfaces were cleaned by sonication in separate baths of acetone, alcohol, and deionized water and affixed with silver paint to the substrate holder/heater stage. The laser output power was controlled by varying the voltage output of its power supply achieving a power density at the target surface of ~4.8 J/cm^2. This power density has been shown previously to allow accurate stoichiometric transfer from target to substrate. [4] Each sample included 36,000 laser pulses resulting in a ~500 nm *BaM* film.

Task 2: Characterization of the Chemistry, Structure and Defects of Buried Interfaces

Samples were characterized for phase purity and crystallographic texture, microstructure, atomic structure, surface morphology, and composition. Cross sectional imaging and analyses included evaluation of chemistry, phase and structure of interface regions. DC magnetic and RF properties were measured and correlated with data gleaned from the above measurements. Investigative techniques included x-ray diffractometry (XRD) including pole figure analyses, atomic force microscopy (AFM), x-ray reflectivity, scanning electron microscopy (SEM) and high-resolution transmission electron microscopy (HR-TEM), and energy dispersive X-ray spectroscopy (EDXS). Magnetic characterization was performed using vibrating sample magnetometry (VSM) whereas RF characterization was performed by the measurement of ferromagnetic resonance (FMR) following the methodology of ref. [5]. FMR measurements were carried out using a vector network analyzer (VNA) at a frequency of 45 GHz. High frequency losses are presented as the FMR

linewidth (ΔH_{FMR}), sometimes referred to as the gyromagnetic resonance linewidth, that has a direct impact upon the insertion loss of circulators and isolators.

Figure 1 is a representative room temperature $\theta - 2\theta$ X-ray diffraction pattern from a *BaM* film grown on MgO/AlN/SiC(Si-polar). The spectrum, in which the diffracted intensity is plotted on the logarithmic scale, illustrates (00l) reflections from the BaM, AlN, and SiC phases with additional low-intensity reflections from the MgO (111) nucleation layer. No other diffraction features rise above the ~1% intensity threshold relative to the BaM (008) peak. The inset to Figure 1 contains pole figures acquired along the <008> and <110> directions. These confirm the epitaxial nature of the BaM film having c-axis-oriented grains (<008>) and 6-fold in-plane registry (<110>) expected from hexagonal crystals, respectively.

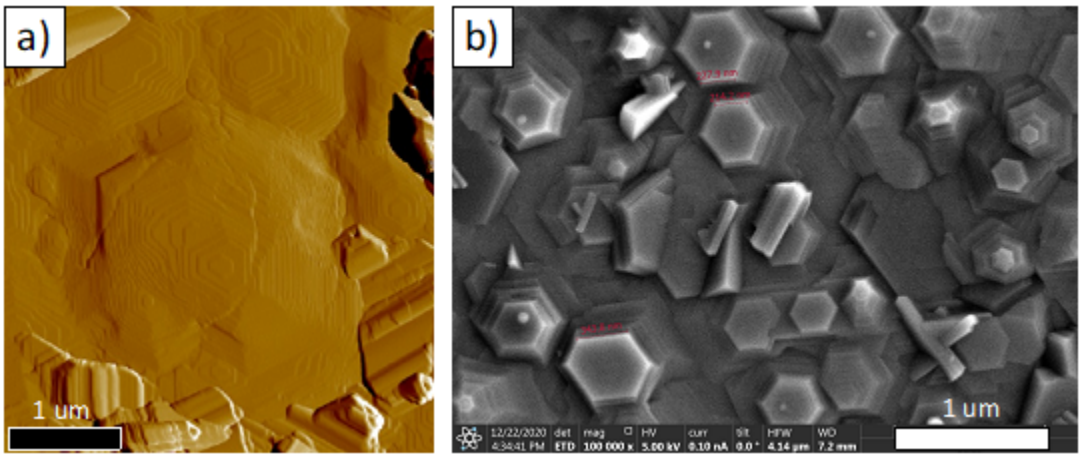

Figure 2. (a) Atomic force microscopy image of the surface of the BaM/MgO/AlN/SiC(X) heterostructure (where X indicates SiC is a single crystal substrate). Hexagonal crystals are seen with fine structure supporting the existence of step-flow growth terraces. (b) Scanning electron microscopy image of the same sample depicted in (a). Many adjoining faceted grains of hexagonal symmetry with crystallographic c-axes normal to the substrate plane exist again with terraces clearly visible.

Figures 2 (a) and (b) are AFM and SEM images, respectively, of the surface morphology of the sample whose XRD data are presented in Figure 1. Here, one observes 0.5-1 μm diameter grains with visible hexagonal facets oriented with c-axes normal to the sample plane. This is also observed in the panel (b) SEM image. Close inspection of both images reveals the presence of terraces.

PLD film growth typically takes place by step-flow and/or Stranski–Krastanov (SK) mechanisms.[6] Step-flow growth occurs when substrate temperatures are sufficiently high to allow migration of surface adatoms to form terraces. Such features are typically smooth and of high crystalline quality. Continued growth often leads to the stacking of terraces that are clearly visible in Figure 2.

Alternatively, SK growth consists of an initial 2D growth, in this case likely associated with a step-flow mechanism, before transitioning to 3D island growth. 2D terraces of the growing film act as templates for the nucleation of 3D islands. Nucleation is triggered by the accumulation of stacking faults that form to accommodate stress resulting from the atomic lattice mismatch between the *BaM* film and the heterostructure template.

The images of Fig. 2, together with the X-ray diffraction spectrum and pole figures of Fig. 1, confirm growth mechanisms and the epitaxial nature of *BaM* films on select WBG heterostructures presented here.

Figures 3 (a-e) are a composite of transmission electron microscopy images and fast Fourier transforms (FFT) of the heterostructure cross section. Panel (a) is illustrative in that it illustrates five distinct regions: (i) the AlN capping layer (∼50 nm) on SiC (Si-polar), (ii) an amorphous-like diffusion region of Al_2O_3 (∼45 nm) that forms between AlN and MgO, (iii) a crystalline nucleation layer of MgO (32 nm) with (111) crystallographic orientation, (iv) a diffusion region between the MgO and BaM forming $MgFe_2O_4$ (∼40 nm), and (v) a highly crystalline thick film of *BaM*. Panel (b) is an expanded HR-TEM view of the *BaM* film structure showing a near perfect arrangement of parallel atomic planes defining the length of M-blocks to be 1.186 nm. This value is consistent with values reported by others (e.g., 1.16 nm [7]). From these data, *BaM* lattice parameters of a=b=0.601 nm and c=2.366 nm were deduced. Based on these calculations, a and c lattice parameters experience a ∼2% dilation relative to published bulk *BaM* values of a=b=0.58876 nm and c=2.31885 nm.[8] However, these values reflect the atomic structure nearest the interface region where strain is most pronounced. The in-plane lattice parameter of the *BaM* film >50 nm above the interface region indicates lattice parameters of a=b=0.5873nm reflecting a slight compressive strain of ∼0.3%, and a constant *c* parameter of 2.366 nm which maintains the aforementioned tensile strain of 2%. Figure 4 illustrates the transition from the $MgFe_2O_4$ spinel layer to the hexaferrite phase that includes a large mismatch in lattice parameters ($a_{MgFe_2O_4} = 0.836\,nm$)[9] providing a considerable strain field. This transition triggers the formation of stacking faults. The accumulation of copious stacking faults in the immediate region above the interface of the spinel interdiffusion layer and the *BaM* film is clearly visible. The stacking fault region extends to about 30 nm above the interface. Beyond this region stacking faults are no longer detected in large numbers.

These atomic characteristics for *BaM* film growth suggest in-plane strain is relieved as the BaM grows thicker, a common observation in heteroepitaxial growth. Alternatively, the out-of-plane strain remains unchanged. This behavior has been attributed by others to the presence of oxygen deficiencies in the *BaM* film.[11]

Figures 5 (a-d) are hysteresis loops for heterostructures whose comparison proves illustrative in relating sample structure and chemistry to magnetic properties. In Figure 5 (a) are hysteresis loops for the BaM/MgO/AlN/SiC(X) sample that show clear magnetic anisotropy with an anisotropy

field (H_a) of ~16.5 kOe and a saturation magnetization ($4\pi M_s$) of 4.2 kOe. These values are very near published values for bulk *BaM* materials, i.e., 17 kOe and 4.3 kG, respectively.[26] Similar loops are presented for heterostructures without the AlN capping layer and for a BaM/Pt/SiC(X) heterostructure. For the BaM/MgO/SiC(X) sample (Fig. 5 (b)), loops collected for both in-plane and out-of-plane directions nearly overlap indicating very little magnetic anisotropy and a low H_a (that is difficult to quantify merely by inspection). Also, the saturation magnetization, as $4\pi M_s$, is 1.7 kG, or 62% lower than the BaM/MgO/AlN/SiC(X) sample. Electron microscopy characterization of this sample showed a lack of epitaxy and a microstructure dominated by misoriented grains that did not coalesce during growth indicating the important role of the capping layer in passivating the SiC surface. Figure 5 (c) shows a comparison of loops collected from a sample similar to that presented in panel (b) where the nucleation layer has been replaced by Pt. In this sample, the anisotropy is smaller than (a), and the magnetization reflects porosity that was confirmed by SEM and TEM studies. Finally, panel (d) illustrates hysteresis loops collected from the BaM/MgO/GaN/Sapphire(X) heterostructure in which the saturation magnetization is near the bulk value. However, electron microscopy reveals a nonuniform film surface with grain outgrowth that induces surface pinning of domain walls resulting in a high coercivity (H_c) of >2 kOe. The high coercivity positively impacts squareness, $Sq = \frac{M_r}{M_s}$, which reaches 0.70 but degrades ΔH_{FMR} by >60% over the BaM/MgO/GaN/SiC(X) heterostructure value of 340 Oe. The latter reflects the role of porosity in FMR linewidth. Specifically, the contributions to FMR linewidth in our samples by magnetic anisotropy is reflected in Schlömann's expressions as $\Delta H_{anis} = 1.08J\left(\frac{H_A^2}{4\pi M}\right)$ and from porosity as $\Delta H_{poros} = 0.502J4\pi M(p)$ [12] where H_A is the anisotropy field ($2\frac{K_u}{M}$), p is the porosity of the material ($\sim 0.04 \pm 0.02$), J is a shape factor 0.89 (factor of N_Z=0.95) [13] and $4\pi M_s$=4210 G.

We estimate ΔH_{anis}= 58 Oe and ΔH_{poros}=75 Oe from which ΔH_{total}=133 Oe. The measured linewidth was 340 Oe. This leaves 207 Oe of dynamic loss related to two-magnon scattering. Such a loss mechanism arises from the interaction of spin waves with impurities or discontinuities such as grain boundaries or triple junctions giving rise to energy loss to the media. In our cases, this would be through interactions with one- and two-dimensional defects (e.g., stacking faults), interfacial discontinuities in structure and chemistry, and at grain boundaries. Defects giving rise to two-magnon scattering are often responsible for DC hysteretic losses in the form of high H_c. In our samples, Hc values approach or exceed 1 kOe supporting this assertion.

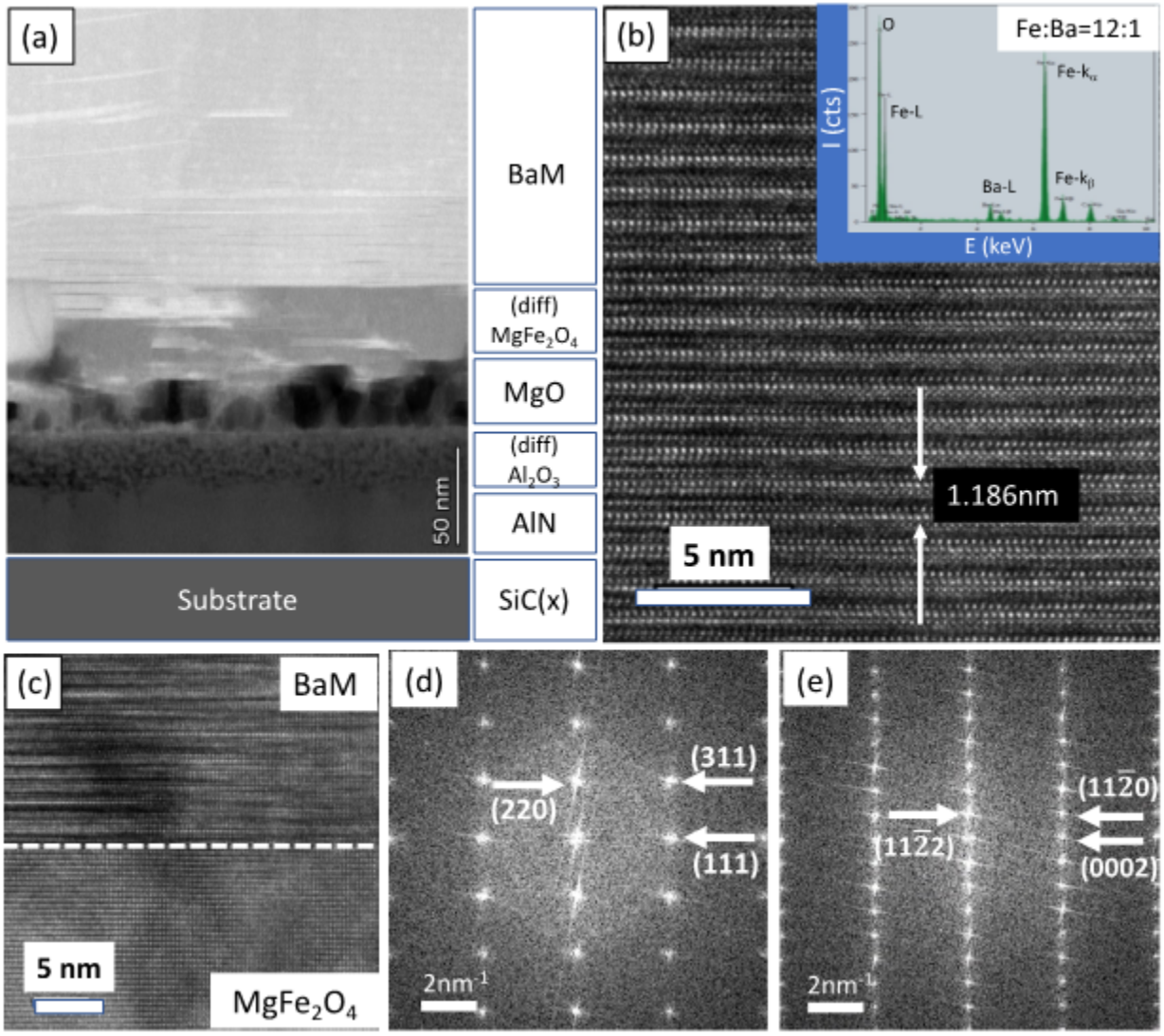

Figure 3. (a) Cross section transmission electron microscopy image of the BaM/MgO/AlN/SiC(X) heterostructure revealing five distinct regions as denoted to the right hand side of (a). (Note: "diff" indicates a diffusion region.) (b) Expanded view of the BaM film cross section revealing parallel stacking of M-blocks with individual dimension 1.186 nm. Inset to this panel is an energy dispersive x-ray spectrum confirming the nominal stoichiometric ratio of Fe:Ba = 12:1. (c) Expanded view of (a) at the BaM/MgO interface where a well-ordered region forms having the $MgFe_2O_4$ phase. (d) The FFT pattern of the interdiffusion region of that depicted (c) and (e) the FFT pattern of the deposited *BaM* layer.

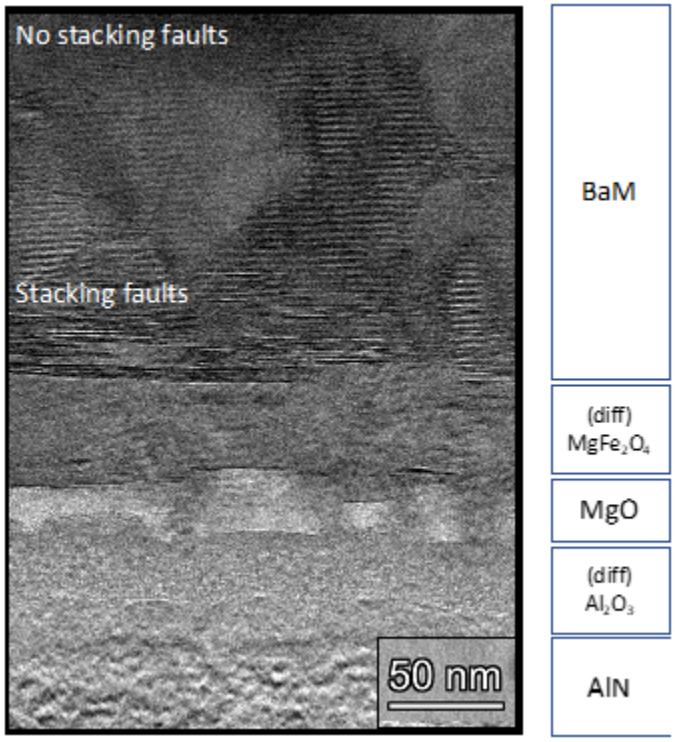

Figure 4. Cross section transmission electron microscopy image revealing distinct regions of the BaM/MgO/AlN/SiC(X) heterostructure as denoted on the right-hand side. Stacking faults are clearly visible in the first 30 nm of *BaM* film growth on the $MgFe_2O_4$ diffusion region.

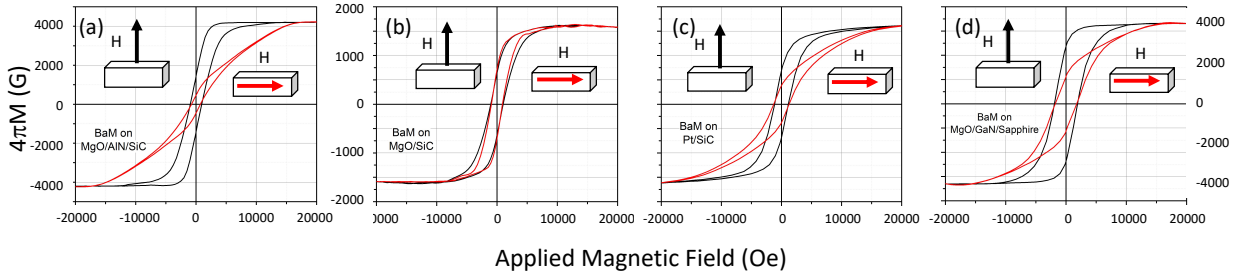

Figure 5. Hysteresis loops, as sample magnetization (4πM, G) versus applied magnetic field (H) where the applied field is scanned from 0 Oe to $\pm$ 20 kOe (beyond the magnetic saturation field of ≅17 kOe), are presented for three heterostructure samples. Inset graphics define the orientation of the applied magnetic field relative to the substrate axes. (a) Hysteresis loops collected from the BaM/MgO/AlN/SiC(X) sample, (b) similar data collected for a heterostructure without an AlN capping layer, (c) loops collected from a BaM/Pt/SiC(X) sampled), and (d) loops collected from BaM/MgO/GaN/Sapphire(X).

Table 1. Structure and magnetic properties of BaM films grown on WBG-based heterostructures.

Heterostructure	H_A (kOe)	H_c (kOe)	$\frac{M_r}{M_s}$	ΔH_{FMR} [a] (Oe)	$4\pi M_s$ [b] (kG)	Comments
BaM Bulk Reference [14] (crystal textured poly-X)	17.0	0.45	0.88	1250	3.60	H_c $Sq = \frac{M_r}{M_s}$, and FMR linewidth (ΔH_{FMR}) are highly sensitive to the effects of processing, e.g., porosity and grain orientation, and may vary from study to study.
BaM/MgO/AlN/SiC(X) (Si-polar)	16.5	0.93	0.32	400	4.21	(see text for discussion)
BaM/MgO/AlN/SiC(X) (C-polar)	15.0	1.50	0.38	c)	3.65	BaM films deposited on C-polar SiC shows 10% lower anisotropy and 13% lower saturation magnetization compared with Si-polar SiC heterostructures. The degradation of properties results from the lack of crystallographic texture in the MgO layer that also experienced a nearly 5 times larger surface roughness.
BaM/MgO/SiC(X)	d)	1.10	0.30	c)	1.58	Saturation magnetization is 62% lower than the BaM/MgO/AlN/SiC(X) sample. Electron microscopy reveals a lack of epitaxy and a microstructure dominated by misoriented grains that did not coalesce during growth resulting in high porosity. A 100 nm thick SiO_2 forms on the SiC where Mg and Si combine with elements present to form perovskite and spinel phases.

BaM/Pt/SiC(X)	15.5	1.22	0.50	c)	3.22	Pt layer is shown to be an effective nucleation layer limiting interdiffusion between the BaM film and SiC substrate. However, upon high temperature growth, Pt forms discontinuous multiphase (i.e., $BaFeSi_4O_{10}$ and Fe_3O_4) islands in the interdiffusion region.
BaM/MgO/GaN/SiC(X)	15.5	1.16	0.35	340	3.20	GaN shows the potential as an effective SiC capping layer for BaM film growth. Lower anisotropy fields and saturation magnetization values indicate the misalignment of crystals and presence of porosity.
BaM/MgO/GaN/Sapphire(X)	15.6	2.10	0.70	550	4.00	Electron microscopy reveals a nonuniform film surface and grain outgrowth that induces surface pinning of domain walls resulting in higher magnetic coercivity (H_c).

Notes:
(X): single crystal substrates
(poly-X): polycrystalline BaM materials
a) ΔH_{FMR} is measured as the peak-to-peak of the power derivative
b) $4\pi M_s$ is determined by the VSM measured value of magnetization in emu normalized to the sample volume defined as sample area multiplied by deposited *BaM* layer thickness resulting from 36,000 laser pulses
c) No clear FMR detected in these samples
d) No significant magnetic anisotropy observed in these samples

Task 3: Correlation of measured interface properties with functional properties

Table 1 presents quantifiable magnetic properties where measurements permitted.

By inspection of Table 1, one observes the highest quality sample to be of the BaM/MgO/AlN/SiC(X, Si-polar). An identical sample with C-polar termination of the SiC substrate being the only difference led to an AlN capping layer having five times the average surface roughness of the Si-polar termination. This led to an overall degradation of crystal quality and magnetic properties (i.e., 61% increase in coercivity, 13.3% reduction in saturation magnetization and lack of magnetic anisotropy). The causal relationship between C- versus Si-termination and their chemical affinity to the AlN capping layer remain ambiguous. The BaM/MgO/GaN/SiC(X) heterostructure is characterized as having the lowest ΔH_{exp}=340 Oe and near bulk-like anisotropy field. However, its saturation magnetization is 24% lower than the best sample, signally high porosity or extensive interfacial alloying. All samples had hysteresis loop

squareness values below 50%. At these values, the structures lack self-bias properties. Lacking self-bias properties does not preclude their use in circulators but it does require the use of a bias magnet. An exception is the BaM/MgO/GaN/Sapphire(X) heterostructure. This structure has a squareness of 70% and a saturation magnetization approaching bulk-like values. However, the static and dynamic loss properties of this structure are higher than representative industrial material standards.

Conclusions

In summary, presented here are results of a systematic study of PLD grown *BaM* films on industrial-compatible WBG semiconductor heterostructures suitable for operation in Ka-band circulators. *BaM* films having device quality performance in structure, epitaxy, and magnetic properties were realized for BaM/MgO/AlN/SiC(X) heterostructures. Film properties include near bulk-like values of magnetic anisotropy field, $H_a \sim 16.5$ kOe, and saturation magnetization, $4\pi M_s \sim 4.2$ kG. FMR linewidth values are consistent with device design goals for insertion loss and other device performance metrics. Heterostructures where SiC substrates having Si-polar termination show particular promise whereas C-polar surfaces give rise to high and detrimental average roughness leading to the deterioration of RF performance. Overall, hysteresis loop squareness values remain low for self-bias applications. Prior work has shown that reducing dynamic losses (two-magnon scattering) while maintaining static losses (domain wall pinning) is one path to realizing high squareness and low linewidths.[15]

These results provide an important first step in the integration of active and passive components on a single wafer essential to the realization of a transmit/receive system on wafer (*SoW*) topology necessary for the development of 5G Ka-band massive multiple input – multiple output (*m-MIMO*) antenna arrays with true full duplexing in time and frequency domains.

References

1. Z. Chen and V.G. Harris, “Ferrite Film Growth on Semiconductor Substrates Towards Microwave and Millimeter Wave Integrated Circuits,” J. Appl. Phys. 112, 081101 (2012).

2. C. Yu, A.S. Sokolov, P. Kulik, V.G. Harris, Stoichiometry, phase, and texture evolution in PLD-Grown hexagonal barium ferrite films as a function of laser process parameters, J. Alloy. Compd., 814 152301 (2020).

3. M. Xiao, Z. Du, J. Xie, E. Beam, X. Yan, K. Cheng, H. Wang, Y. Cao, and Y. Zhang, “Lateral p-GaN/2DEG junction diodes by selective area p-GaN trench-filling-regrowth in AlGaN/GaN,” Appl. Phys. Lett., 116, 053503 (2020).

4. A.S. Sokolov, M. Geiler, V.G. Harris, “Broadband ferromagnetic resonance linewidth measurement by a microstrip transmission resonator,” Applied Physics Letter, 108, 172408 (2016).

5. V. Harris and Z. Chen, U.S. patent 8,029,921, “Growth of high quality low-loss ferrite materials on wide bandgap semiconductor substrates,” 2011.

6. J. Venables, Introduction to Surface and Thin Film Processes. Cambridge: Cambridge University Press, 2000.

7. C. Sudakar, G.N. Subbanna, and T.R.N. Kutty, “Wet chemical synthesis of multicomponent hexaferrites by gel-to-crystallite conversion and their magnetic properties,” J. Magn. Magn. Mater., 263, 253 (2003).

8. R.C. Pullar, “Hexagonal ferrites: A review of the synthesis, properties and applications of hexaferrite ceramics,” Progress in Materials Science, 57, 1191 (2012).

9. S. Verma, P.A. Joy, Y.B. Khollam, H.S. Potdar, S.B. Deshpande, “Synthesis of nanosized MgFe2O4 powders by microwave hydrothermal method,” Materials Letters, 58, 1092-1095, (2004).

10. Z. Xu, Z. Lan, G. Zhu, K. Sun, and Z. Yu, “Effects of the oxygen partial pressure during deposition on the material characteristics and magnetic properties of BaM thin films,” J. Alloy. Compd., 538, 11 (2012).

11. H. Kojima, Ferromagnetic Materials, edited by E. P. Wohlfarth, North Holland, New York, 1982, Vol. 3.

12. E. Schlömann, “Spin-wave analysis of ferromagnetic resonance in polycrystalline ferrites,” J. Phys. Chem. Solids 6, 242 (1958).

13. S. Geschwind and A. M. Clogston, “Narrowing effect of dipole forces on inhomogeneously broadened lines,” Phys. Rev. 108, 49 (1957).

14. Yue Dai, Zhongwen Lan, Zhong Yu, Ke Sun, Rongdi Guo, Guohua Wu, Xiaona Jiang, Chuanjian Wu, Yu Liu, Hai Liu, Wei Tong, “Effects of La substitution on micromorphology, static magnetic properties and low ferromagnetic resonance linewidth of self-biased M-type Sr hexaferrites for high frequency application,” Ceramics International, 47, 8980-8986 (2021).

15. Z. Chen, A. Yang, K. Mahalingam, et al., “Structure, magnetic, and microwave properties of thick Ba-hexaferrite films epitaxially grown on GaN/Al2O3 substrates,” Appl. Phys. Lett., 96, 242502 (2010).

Appendix A: Supplemental Data